Structural Insights into the NAD(P)H:Quinone Oxidoreductase from *Phytophthora capsici*

Cancan Yang, Zhenling Huang, Xiuguo Zhang, and Chunyuan Zhu*

ACCESS | Metrics & More | Article Recommendations | Supporting Information

ABSTRACT: Soluble quinone oxidoreductases catalyze transfer of electrons from NADPH to quinones. Transfer of electrons is essential for detoxification of synthetic compounds. Here, we present the crystal structure of a NADPH-dependent QOR from *Phytophthora capsici* (*Pc*) complexed with NADPH at 2.4 Å resolution. The enzyme exhibits a bi-modular architecture, containing a NADPH-binding groove and a substrate-binding pocket in each subunit. In the crystal, each asymmetric unit of *Pc*QOR contains two molecules stabilized by intermolecular interactions. Gel filtration and ultracentrifugation analyses reveal that it functions as a tetramer in solution. Alignment of homologous structures exhibits a conserved topology. However, the active sites vary among the homologues, indicating differences in substrate specificities. Enzymatic assays indicate that *Pc*QOR tends to catalyze the large substrates, like 9,10-phenanthrenequinone. Computational simulation associated with site-directed mutagenesis and enzymatic activity analysis declares a potential quinone-binding channel. The ability to reduce quinones probably helps *P. capsici* to detoxify some harmful chemicals encountered during invasion.
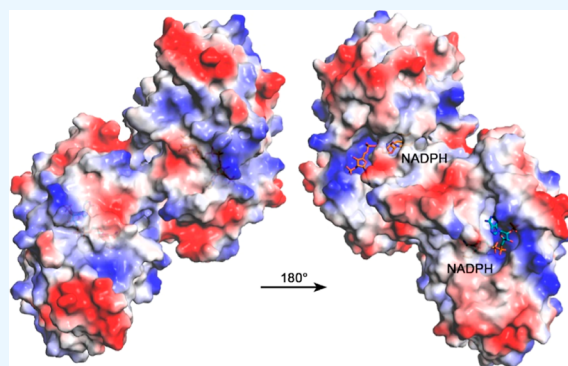
INTRODUCTION

Quinone oxidoreductases (QORs) are a class of enzymes that catalyze the reduction of quinones to hydroquinones. Most quinones are classified as cytotoxic molecules widely distributed in all living organisms.[1,2] QORs could prevent cells from quinone cytotoxic damage, such as reducing the formation of DNA adducts and lipid peroxides.[3−6] QORs are classified into two groups depending on cellular localization: (a) membrane-bound QORs that participate in the respiration chain and generation of energy[7,8] and (b) soluble QORs that reduce quinones to hydroquinones.[9] Soluble QORs play a central role in detoxifying quinones by reducing them to corresponding hydroquinones, which may conjugate to either sulfate or glucuronic acid for excretion.[10−13] Oxygen can react with hydroquinones and lead to consumption of redundants from cells and lipid peroxidation.[11,12,14,15] Most QORs exhibit flexible substrate specificities and catalyze various-size quinones.[9,10] Significantly, the electron-donating ability of QORs is beneficial to degrade organic contaminants.[16]

Soluble QORs are categorized into two groups based on their respective reductive mechanism.[17] DT-diaphorases (EC 1.6.99.2) belong to two-electron reductive enzymes and require FAD as an additional prosthetic group.[15,18] On the other hand, zeta-crystallin-like QORs catalyze one-electron reduction of certain quinones (benzoquinones, naphthoquinones, phenanthrenequinones, and related derivatives) using NADPH as the only cofactor.[19−22] Zeta-crystallin-like QORs belong to the medium-chain dehydrogenase/reductase super-

family,[23,24] which is divided into two subfamilies: zinc-dependent dehydrogenases[25] and non-metallic reductases.[5] *Pc*QOR belongs to the latter class, not requiring zinc ions for catalysis. Zeta-crystallin has been found at low levels in the liver and kidney tissues of both humans and guinea pigs,[26,27] suggesting a metabolic role in the detoxification of quinones.[28] *Phytophthora capsici* encounters harsh conditions during infection, including oxygen deprivation. Perhaps *Pc*QOR participates in generating energy to accept electrons in the absence of oxygen.

So far, the zeta-crystallin-like QORs have been determined in many organisms, such as *Pseudomonas syringae*,[9] *Saccharomyces cerevisiae*,[10] *Thermus thermophilus* HB8,[29] *Escherichia coli*,[17] *Arabidopsis thaliana*,[30−32] *Homo sapiens*,[16,33] and *Streptococcus mutans*.[34] Notedly, the QORs from humans and yeast have a novel activity to hydrogenate the double-bond α,β-hydrogenation of 2-alkenals and 3-alkenones.[35] In addition to the enzymatic activity, they can also bind nucleic acids.[36,37] Moreover, these proteins are speculated to bind adenine—uracil-rich elements to regulate transcription.[38] All homologues
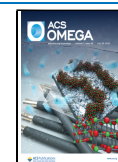
of zeta-crystallin-like QORs exist as dimers in the asymmetric unit.[17] Each subunit contains a catalytic pocket and a cofactor-binding pocket. To delineate the structural differences and mechanism of catalysis between *Pc*QOR and its homologues, we perform structural studies of *Pc*QOR.

Here, we determine the crystal structure of the *Pc*QOR complex with NADPH. The complex structure gives noticeable details of the NADPH-binding interaction. We also investigate the substrate-binding site using computational simulation combined with site-directed mutagenesis and enzymatic activity assays. *Pc*QOR could catalyze both benzoquinone and phenanthrenequinone, emphasizing the need for a flexible active site for detoxifying toxic components encountered by *P. capsici* in the host.

■ MATERIALS AND METHODS

P. Capsici Strain Culture. *P. capsici* LT1534 strain was cultured on oatmeal agar at 25 °C.

Gene Cloning and Protein Purification. The open reading frame of *Pc*QOR (GenBank accession no. OK398115) was amplified from the genomic cDNA of *P. capsici* strain LT1534 using the primer sets described in Supporting Information Table S1 and ligated into the pET28a vector that includes an N-terminal hexahistidine tag.[39] *E. coli* Rosetta cells were transformed with pET28a-*Pc*QOR plasmids and grown in Luria–Bertani medium under kanamycin selection at 37 °C until the A_{600nm} reached 0.8 absorbance units and then induced with 1 mM isopropyl β-D-thiogalactopyranoside at 16 °C for 24 h. The cells were pelleted by centrifugation at 7000*g* for 10 min and then resuspended in resuspension buffer containing 30 mM HEPES, pH 7.5, 150 mM NaCl, and 30 mM imidazole. The cells were subjected to sonication on ice using an ultrasonic homogenizer (Ningbo Scientz Biotechnology Co., Ltd.), and the debris was removed by centrifugation (14,000*g*, 25 min, 4 °C). The supernatant was then loaded onto a Ni-NTA column with an FPLC system (GE Healthcare) equilibrated using lysis buffer and eluted with an elution buffer (30 mM HEPES, pH 7.5, and 150 mM NaCl, followed by a 200–500 mM imidazole gradient), and then washed with 0.5 column volumes of washing buffer. The eluotropic protein was further purified by anion-exchange chromatography with a Resource Q column (GE Healthcare), which was eluted using a linear gradient of NaCl. The protein peak was concentrated to 1 mL and then loaded onto a size exclusion chromatography column (Superdex 200 Increase column, GE Healthcare) pre-equilibrated in 30 mM HEPES, pH 7.5, and 150 mM NaCl buffer. The purified proteins were collected and concentrated to 12 mg/mL. The purity of protein was estimated by SDS-PAGE, and then, the protein was stored at −80 °C for crystallization screening. The mutant proteins were prepared in the same way as the wild-type protein.

Crystallization, Data Collection, Structure Determination, and Refinement. The crystals of *Pc*QOR were grown using the sitting drop vapor diffusion technique and a crystal screen kit (HAMPRON RESEARCH). A 1:1 ratio of protein/reservoir solution was equilibrated against 180 μL of reservoir solution at 10 °C. Crystallization of *Pc*QOR was completed within 3 and 5 days under conditions of 28% v/v 2-propanol, 0.1 M Bis-Tris, pH 6.5, and 3% v/v polyethylene glycol 200. The crystals were directly mounted in a cryoloop and soaked in cryoprotectant solution (20% glycerol) and flash-frozen in liquid nitrogen prior to data collection. All X-ray

diffraction data sets were collected at a radiation wavelength of 0.97 Å on the beam line BL19U at a temperature of 100 K in the Shanghai Synchrotron Radiation Facility (SSRF), China. The diffraction data from *Pc*QOR were collected with the 360° total rotation range, 1° per image, and with the "auto-correction" option in scaling. The "no merge original index" option was used to generate an alternative, unmerged set of data, intended only to calculate correlation coefficients of anomalous difference for two random half sets (CCano) by phenix.anomalous_signal. The data were scaled separately within the 45, 90, 180, 270, and 360° rotation range to analyze the strength of anomalous signals at different multiplicities. The statistics of diffraction data at maximal redundancy are listed in Table 1. All data were processed using HKL3000

Table 1. Data Collection and Refinement Statistics of *Pc*QOR Crystals

	*Pc*OQR
data collection	
space group	P3$_2$21
cell dimensions	
a, *b*, *c* (Å)	84.28, 84.28, 185.605
β (deg)	90.000
resolution (Å)	50–2.40 (2.44–2.40)
R_{merge} (%)	17.9 (42.1)
I/σ	11.19 (5)
completeness (%)	99.9(100)
redundancy	9.0 (9.4)
refinement	
resolution (Å)	2.39
no. of reflections	28,996
R_{work}/R_{free}	17.28 (19.61)/22.74 (29.52)
no. of atoms	
Protein	5287
ligand/ion	96
Water	244
B-factors	35.9
rms deviations	
bond lengths (Å)	0.0086
bond angles (deg)	1.09
Ramachandran plot [%]	
most favored	96.66
additionally allowed	2.62

software.[40,41] The *Pc*QOR structure using the QOR of *T. thermophilus* HB8 (PDB ID 1IYZ) as a search model was solved by molecular replacement (MR) with the Phaser program[42] from the CCP4 suite.[43] Further refinement was carried out by using the programs Phenix[44] and Coot.[45] Ligand fitting maps were performed using the Phenix.ligand fit.[46] 10% of all data set aside was used to calculate R_{free}. Subsequent refinements by incorporating ligands and water molecules were according to the 1.0σ map level. The data collection and refinement statistics are summarized in Table 1. A Ramachandran plot generated with Molprobity indicated that the structure had favorable stereochemistry.[47] High-quality figures of the protein and ligand structures were created with the PyMOL program.[48]

Gel Filtration Assay. Gel filtration assay was performed for analyzing the solution state of *Pc*QOR. A Superdex 200 Increase column was pre-equilibrated with a buffer containing 30 mM HEPES, pH 7.5, and 150 mM NaCl. 2 mg/mL protein
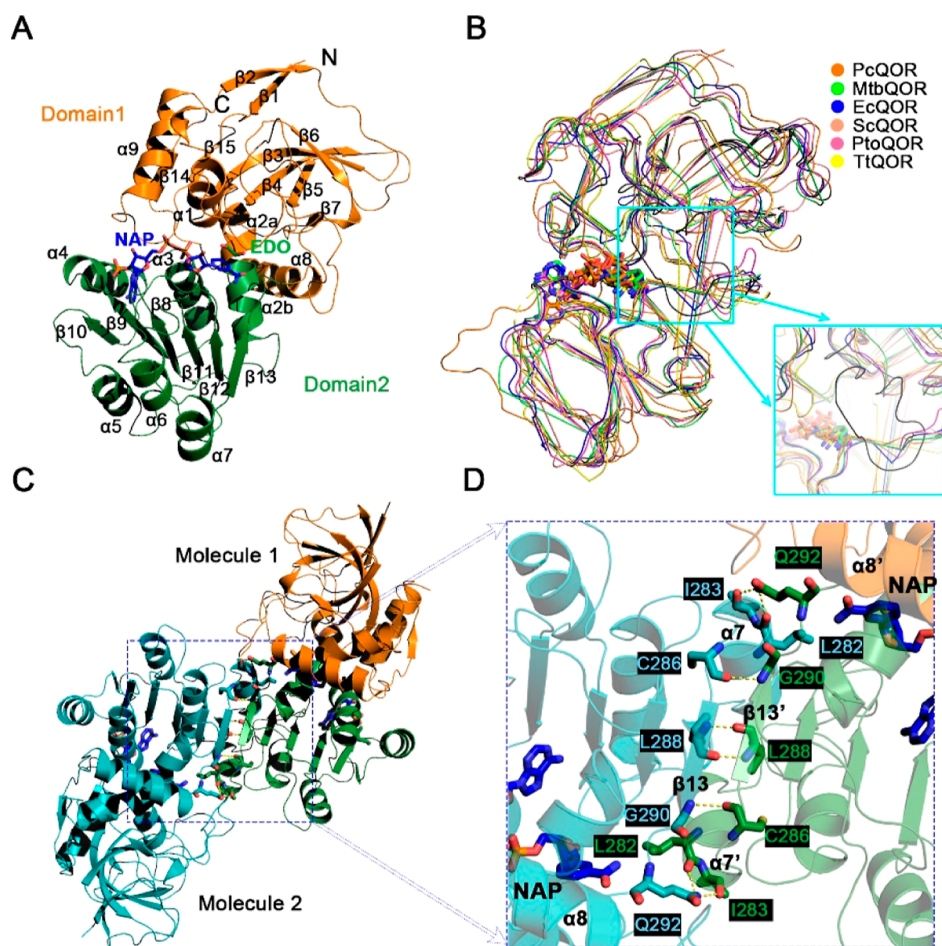
Figure 1. Overall structure of *Pc*QOR. (A) *Pc*QOR−NADPH complex monomer. The monomer is presented as a cartoon model with domain1 being colored orange and domain2 being colored forest. (B) Structural comparison among QORs from various species. *Pc*QOR is shown in orange; *Mtb*QOR (PDB: 4RVU) is shown in green, *M. tuberculosis* quinone oxidoreductase; *Ec*QOR (PDB: 1QOR) is shown in blue, *E. coli* quinone oxidoreductase; *Sc*QOR (PDB: 3QWB) is shown in pink, *S. cerevisiae* quinone oxidoreductase; *Pto*QOR (PDB: 3JYN) is shown in magenta, *Pseudomonas syringae* pv. tomato DC3000 quinone oxidoreductase; and *Tt*QOR (PDB: 1IYZ) is shown in yellow, *Thermus thermophilus* HB8 quinone oxidoreductase. The larger part at the corner exhibits a special loop colored black in *Pc*QOR, acting as a cover over the active pocket. (C) *Pc*OQR dimer. Molecule 1 is colored orange with forest and molecule 2 is colored cyan. Interacting residues between the two subunits are shown as sticks. (D) Larger features are also shown on the right.

of *Pc*QOR was loaded onto the column and eluted under conditions of 30 mM HEPES, pH 7.5, and 150 mM NaCl at a flow rate of 0.5 mL/min. The Bio-Rad's gel filtration standard was used to estimate the molecular weight of the *Pc*QOR multimer.

Analytical Ultracentrifugation. Sedimentation velocity experiments were performed using an Optima AUC analytical ultracentrifuge equipped with two detection systems of ultraviolet light and interference light (Beckman Coulter). 2 mg/mL *Pc*QOR in buffer containing 30 mM HEPES, pH 7.5, and 150 mM NaCl was centrifuged at 4 °C at 42,000*g*, and the *Pc*QOR migration was monitored based on absorbance at 280 nm. The sedimentation velocity data were analyzed using SEDFIT.[49,50]

Computational Docking. The structure of HNQ was acquired from the CYP158A2 complex structure.[51] The structures of 1,2-benzoquinone (NQ) (O═C1C═CC2═C(C═CC═C2)C1═O) and PQ (O═C1C(═O)C2═C(C═CC═C2)C3═C1C═CC═C3) were transformed from the SMILES (simplified molecular input line entry specification) level representations with the program phniex.-elbow.[52] The three computer-simulated structures were

generated using Autodock4.2.6, which is a suite of automated docking tools.[53,54] Each molecule could obtain more than 100 initial poses, for each of which conformation was scored. The optimal pose was scored for van der Waals and electrostatic interactions and was rigid-body-minimized.

Site-Directed Mutagenesis. Variants were constructed using a fast site-directed mutagenesis kit (Tiangen Biotech (Beijing) Co Ltd.) with the wild-type *Pc*QOR plasmid as a template. The sequences of the mutagenesis oligonucleotides are listed in Supporting Information Table S2. The PCR products were incubated with DpnI (Tiangen Biotech (Beijing) Co. Ltd.) to digest the original DNA template and then separately transformed into *E. coli* strain FDM competent cells. Each mutant site change has been confirmed by sequencing.

Activity Assays. The kinetic parameters of enzymes were measured by the previous method.[55] Kinase reactions were carried out in a buffer solution containing 100 mM HEPES, pH 7.5, 100 mM NADPH, 0.1 mg/mL *Pc*QOR, and 0.25 mM substrates at 25 °C. The substrates were dissolved in absolute alcohol with final 2% concentration in the assay. The reaction rate was monitored using NanoPhotometer Pearl by recording
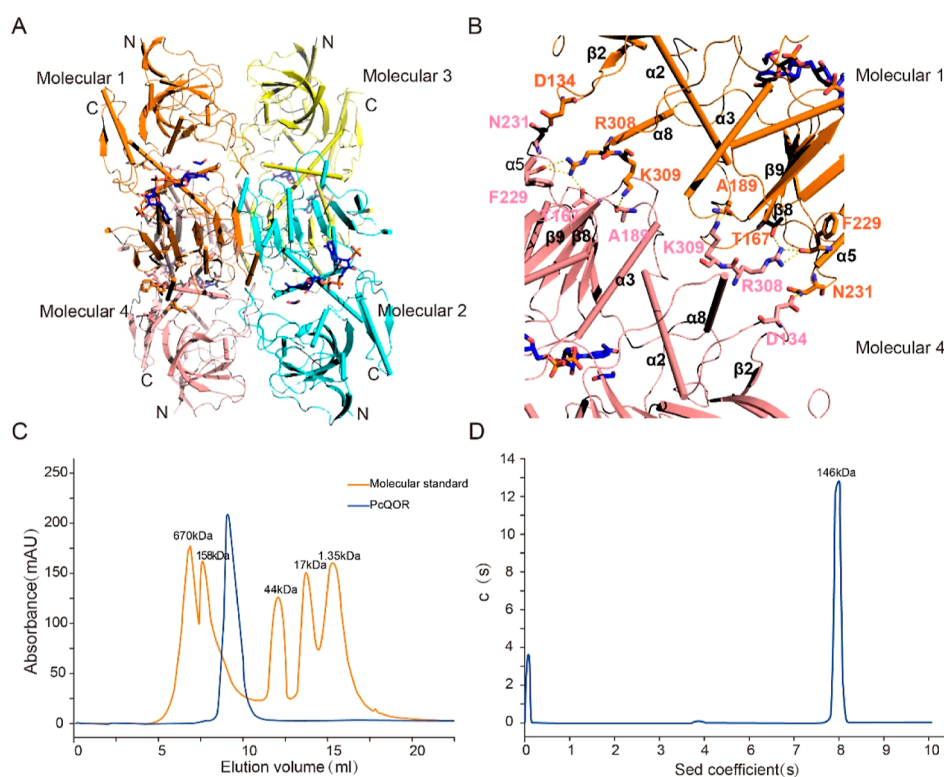
Figure 2. *Pc*QOR functions as a tetramer. (A) The tetramer is presented as a cartoon model. The monomers within the tetramer are shown in different colors. The N- and C-termini of the protein are marked N and C, respectively. (B) *Pc*QOR tetrameric interface. Interacting residues between the tetrameric interfaces are shown as sticks and the helices are shown as cylindricity. (C) Gel filtration analysis shows that *Pc*QOR eluotropic peak spans the expected tetramer volumes. (D) Ultracentrifugation analysis of *Pc*QOR. Sedimentation velocity experiment suggests that *Pc*QOR exists as a tetramer in solution.

the decrease in absorbance of NADPH at 340 nm. The non-enzymatic reduction of NADPH was set as the background control for each assay. The kinetic parameters of mutant enzymes were performed at 25 °C for 15 min.

RESULTS AND DISCUSSION

Overall Structure of PcQOR. We determined the recombinant protein PcQOR crystal structure by MR, which is refined to 2.4 Å resolution (Table 1). In the native structure of *Pc*QOR, ethylene glycol, the smallest component of polyethylene glycol 200, is present in the active site pocket of each monomer. Significantly, judging from the strong difference density peak of definable shape, nicotinamide adenine dinucleotide phosphate (NADPH) is present in the active pocket of each monomer (Figure 1A).

Resembling the other QORs, *Pc*QOR exhibits a bi-modular architecture, which is characterized by two function domains: a catalytic domain (domian1) and a NADPH-binding domain (domain2), which are connected by helix α2. The helix α2 is divided into two segments, labeled α2a and α2b. Domain1 is formed by the N- and C-terminal segments. The N-terminal segment comprises seven β-strands (β1−β7) and the α2a-helix, while the C-terminal segment is composed of two β-strands (β14−β15), an α8-helix, and an α9-helix. These two parts are combined together to form domain1. Significantly, domain1 exhibits a compact bundle, which is formed by strands β3, β4, β5, and β6. Helix α1 is embedded into the bundle. This bundle is in immediate proximity to the NADPH-binding domain; therefore, this motif is very likely to play a pivotal role in substrate binding. Domain2 is formed from

G149 to G294 that folds into a classical Rossmann fold,[56] which is constituted by two $\beta\alpha\beta\alpha\beta$ units flanked by three α-helixes on either side. The long helix α2 horizontally inserts into the protein and links the two domains (Figure 1A).

The overall structure of PcQORs is similar to that of QORs from *P. syringae* pv. tomato DC3000,[9] *S. cerevisiae*,[10] *E. coli*,[17] *T. thermophilus* HB8,[29] and *Mycobacterium tuberculosis*[57] (Figure 1B). In the Dali server,[58] *Pc*QOR retrieved some alcohol dehydrogenases as top hits, suggesting that *Pc*QOR shares a conserved structure with alcohol dehydrogenases. However, the lack of the zinc-binding motifs probably affects interaction between QORs and hydrogen from alcohols. Importantly, there is a long unique loop (90−108) in *Pc*QOR, compared to other homogeneous QORs, covering the region above the active site in *Pc*QOR (Figure 1B). We speculate that this loop probably plays a guarder role in the substrate entry and product release.

Each asymmetric unit contains one homodimeric molecule in *Pc*QOR. The interface of the dimer is mainly mediated by amino acids from the β13-sheet, α7-helix, and two loops between α7 and α8. The interface area of the dimer is 983.3 Å, and the $\Delta_i G$ of the interface is −14.5 kcal/mol. Across the dimeric interface, there is a contiguous parallel β-sheet bundle made up of 12 β-strands, which is flanked by helices on either side (Figure 1C). Amino acids from β13, α7, and loops connecting α7 and α8 form intermolecular interactions, holding the monomers within the dimer together (Figure 1D). Within the interactions, L282 from α7 of one monomer interacts with Q292 of the adjacent monomer, and these two residues are in close proximity to the nicotinamide moiety of
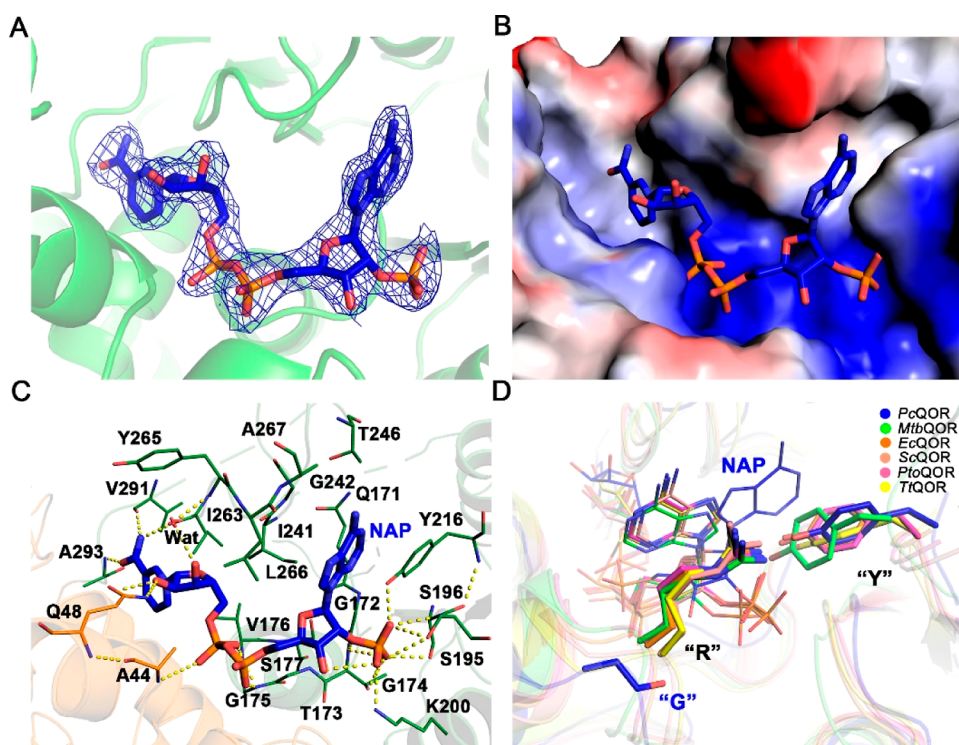
Figure 3. NADPH-interacting network of *Pc*QOR. (A) 2Fo-Fc electron omit map of the NADPH ligand in the *Pc*QOR structure is contoured at 1.0 σ and presented in stereo-view. (B) Electrostatic surface presentation of the NADPH pocket of *Pc*QOR. NADPH is shown as a stick. (C) Enzyme−NADPH interaction network are shown in stereo-view, and the protein residues and NADPH are presented as thin and thick sticks, respectively. (D) Superimposition of NADPH of *Pc*QOR with that of other QORs. NADPH of *Pc*QOR is colored blue, NADPH of *Mtb*QOR is colored green, NADPH of *Ec*QOR is colored orange, NADPH of *Sc*QOR is colored pink, NADPH of *Pto*QOR is colored magenta, and NADPH of *Tt*QOR is colored yellow.

NADPH. Therefore, they are likely to play an important role in assisting in the co-factor for catalysis. Further enhancement of the dimer interface is accomplished through interactions of I283, C286, and L288 from one monomer with Q292, G290, and L288 from another monomer, respectively. This interaction is indispensable because these structural elements stabilize the boundary of the active site. Thus, dimerization of *Pc*QOR probably facilitates the formation of the ligand-binding pockets. A similar mode of dimerization of QORs has been observed previously.[9,10,17,29]

The results of gel filtration and ultracentrifugation analysis reveal that *Pc*QOR exists as a tetramer in solution. Gel filtration results show that *Pc*QOR eluted as a wide peak close to molecular weight marker 158 kDa (Figure 2C). Ultra-centrifugation demonstrates that the macromolecule has a molecular weight of 146 kDa in solution, which approximately quadruples the weight of *Pc*QOR (Figure 2D). Two dimers screwing together form a tetramer (Figure 2A). Amino acids from the α5-helix, α8-helix, and β8-sheet, combined with residues from the loop that connects α2 with β7 and the loop that connects α3 with β9, form intermolecular interactions that hold the dimers within the tetramer together (Figure 2B). The interface area between molecule 1 and molecule 2 is 643.3 Å, and the $\Delta_i G$ of the interface is −0.5 kcal/mol. Within the tetramer, R308 and R309 from α8 of molecule 1 interact with T167, A189, and F229 of the adjacent molecule 4. Further consolidation of the tetramer interface is achieved via interaction of D134 from one monomer with N231 of another monomer. Thus, the intermolecular interactions of these residues guide the protein tetramerization in the solution.

*Pc*QOR functions in the tetramer conformation, a more compact conformation compared to the dimeric topology, which probably contributes to the formation of catalysis-competent ligand-binding pockets.

NADPH-Binding Site. NADPH binds to the cleft between domain1 and domain2 and embeds in a positively charged cavity (Figure 3A,B). Residues from both domain1 and domain2 participate in tethering the co-factor. The adenine ring of NADPH in PcQOR is wrapped in a groove formed by Q171, Y216, I241, G242, T246, L266, and A267 via van der Waals contacts (Figure 3C). The side chain of Y216 stacks against the adenine ring of NADPH. The phosphate group attached to the adenosine ribose is encompassed by positively charged residues (T173, S195, S196, K200, and Y216). The pyrophosphate moiety establishes three hydrogen bonds with G175-N, V176-N, and A44-N. The interaction of the ribose sugar with the protein is perceived by the C2 hydroxyl oxygen with the side chain of Q48 and by the C3 hydroxyl oxygen with the main chain of Y265 through a water atom. The nicotinamide moiety fits into a more open cavity and forms strong interactions with I263-O, V291-O, and A293-N. These interactional amino acids enhance and orient the co-factor optimally for catalysis and provide an applicable binding environment for NADPH.

Superposition of the PcQOR with other homologues reveals that the adenine ring of NADPH in PcQOR exhibits a mirrored orientation compared to NADPH from other species. We speculate that this mirrored conformation of the adenine ring contributes to a more stable NADPH because no additional NADPH molecules were added during cell culture
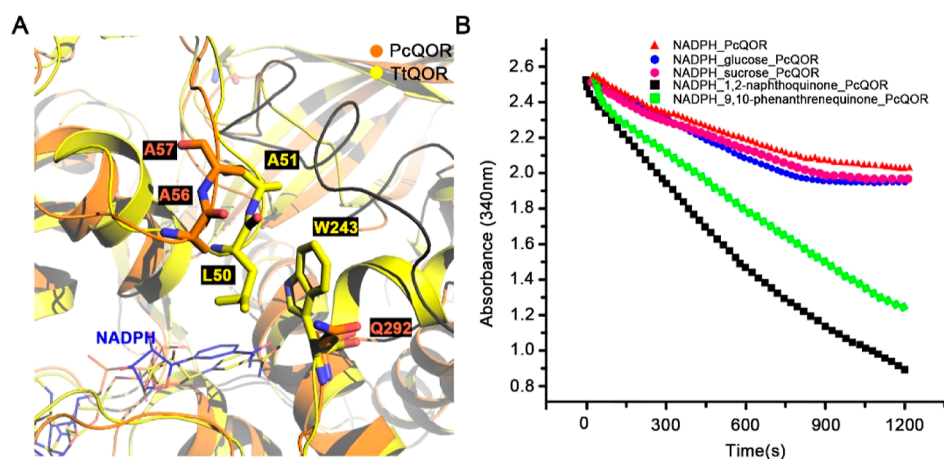
Figure 4. Substrate entrance pocket and enzymatic activity of *Pc*QOR. (A) Superimposition of the substrate entrance pocket between *Tt*QOR in yellow and *Pc*QOR in orange. (B) *Pc*QOR enzyme activity against PQ and NQ was tested by monitoring the absorbance decrease of NADPH at 340 nm. Each measurement was conducted in triplicate under identical conditions.

and crystallization. The different conformation of NADPH may be attributed to the different residue composition in the adenine ring-binding cavity. In QOR homologies, there is an Arg stacking against the adenine ring of NADPH, while in PcQOR, Arg is replaced with Gly and Tyr plays an important role in stacking against the adenine (Figure 3D). Perhaps it is the difference in the nucleotide-binding residues causing the conformational change of NADPH in PcQOR. The unique orientation of NADPH in PcQOR may be relevant to the species specificity. BLAST analysis of the MtbQOR against other oomycetes revealed some orthologues from *Phytophthora palmivora*, *Saprolegnia parasitica,* and *Aphanomyces astaci*. Sequence alignment shows that these three QORs also contain Tyr around the NADPH pocket, while Arg is replaced with Gly or Ser in the NADPH pocket (Figure S1). Side chain of "Glu" or "Ser" residue may be too short to stabilize the adenine ring. Therefore, we surmise that unique orientation of NADPH could be found in QORs of some oomycetes species.

Enzymatic Assays. In *T. thermophilus* HB8 QOR, the entrance to the substrate-binding pocket is blocked by nearby residues L50, A51, and W243, which explains why the large substrates such as phenanthrenequinone cannot be reduced.[29] In contrast, the access to the substrate-binding pocket in PcQOR, which is guarded by nearby residues A57, A56, and Q292, exhibits greater opening for substrates compared to *T. thermophilus* HB8 QOR. A57, A56, and Q292 locate above the nicotinamide moiety and establish a large opening through which NADPH may accomplish the hydride transfer (Figure 4A).

To characterize the enzymatic activity of PcQOR, we determined the enzymatic activities against substrates such as NQ and 9,10-phenanthrenequinone (PQ) kinetics. PcQOR catalyzed PQ more efficiently than NQ. Additionally, we measured glucose and sucrose in the presence of Zn^{2+} as substrates of PcQOR in activity assays. Despite sharing conservative topology between QORs and alcohol dehydrogenases, PcQOR did not show a significant effect of sugar compounds (Figure 4B). The characteristics of the substrate-binding site in the PcQOR–NADPH structure may provide some insights into the specificity of the enzyme for different substrates.

Putative Binding Sites of HNQ, NQ, and PQ in the Substrate-Binding Pocket. Upon NADPH binding, QORs

catalyze transfer of electrons from NADPH to substrates.[56] The C4 atom in the nicotinamide ring of NADPH is the key site where electron transfer occurs. Thus, the substrate-binding site is speculated to be located in the groove between the nicotinamide ring and domain1. We examine the region around the C4 atom of the nicotinamide moiety to acquire information about the substrate-binding site. The electrostatic potential surface of PcQOR–NADPH indicates that the substrate-binding site is located in a region surrounded by polar residues, which construct two sidewalls. The hydrophilic sidewall is composed of N43, R45, D46, Q48, Y54, S67, D68, C147, T148, and K341 from domain1, while the hydrophobic sidewall consists of V176, A293, and NADPH. Importantly, C147, T148, and V176 are within 5 Å of the C4 atom of the NADPH nicotinamide moiety. In addition, ethylene glycol is found in the substrate-binding pocket, held tightly by hydrogen bonds to the protein and NADPH (Figure 5A).

We failed to acquire crystals of the PcQOR tertiary complex with NADPH and ortho-quinones. Therefore, we docked two classical ortho-quinone substrates, PQ and NQ, and one typical ortho-quinone product, HNQ to the PcQOR–NADPH complex using the program Autodock4.2.6.[53] Docking produced 10 clusters for PQ, NQ, and HNQ, respectively. For every docking substrate, we picked out the lowest-energy restraint, which is packed parallel to the nicotinamide ring. The carbonyl groups of quinone of HNQ and NQ point outward the N43, R45, Q48, C147, T148, and K341, while the carbonyl groups of quinone of PQ pointed inward the N43, R45, Q48, C147, T148, and K341. Importantly, all three molecules stack between NADPH and Y54. One carbonyl oxygen atom of HNQ and NQ interacts with the side chain of Y54 through a hydrogen bond, and the other carbonyl oxygen is stabilized by the C2 hydroxyl oxygen atom of the nicotinamide ribose and the side chain of Q48 (Figure 5B–D). Thus, we deduce that the polar residues in the active pocket create an ideal environment for catalysis.

Site-Directed Mutagenesis of PcQOR. To confirm the docking results, we detect the catalytic activities of mutants of R45, Q48, Y54, C147, and T148, which exhibit a stronger affinity to substrates predicted from the above docking pattern. The result discriminates that the five amino acids are essential for substrate binding (Figure 6). R45, Q48, and Y54 are predicted to stabilize the carbonyl group of the substrates. As
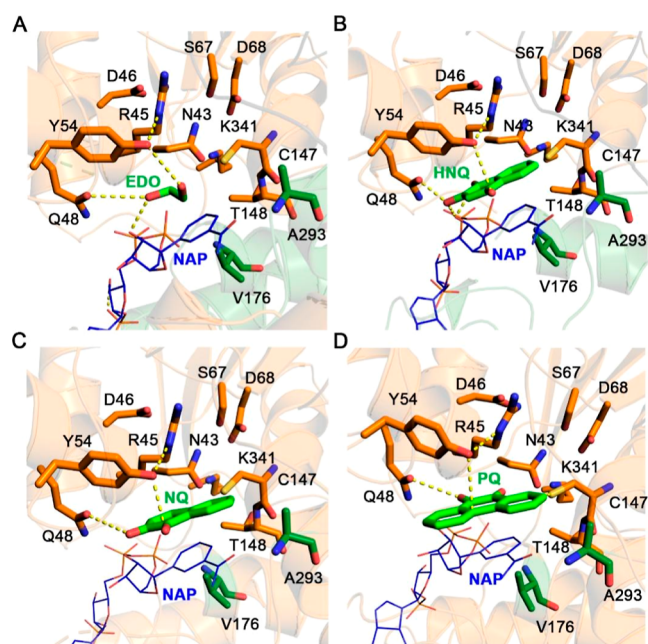
Figure 5. Docking of HNQ, NQ, and PQ to (A) *Pc*QOR−NADPH complex. Ethylene glycol and active residues of the interaction network are shown as sticks. Docking pattern of (B) HNQ, (C) NQ, and (D) PQ to *Pc*QOR. Ligands and active residues are shown as sticks. NADPH colored blue is shown as a line. Distances <4.0 Å are indicated with dashed lines.

shown in Figure 6, the enzyme activities of the three mutants are very low, indicating that residues R45, Q48, and Y54 are essential for catalytic activity. C147 and T148 are predicted to form hydrogen bonds with the phenyl rings of ortho-quinones. Variants of these two amino acids show an almost complete loss of enzyme activity. All these imply that these five residues play an important role in shaping a suitable environment for catalysis of substrates. Although N43, D46, S67, D68, V176, and K341 are predicted to surround the substrate, mutations of these residues result in inapparent loss of activity. All these

show that simulation of complex structures could provide important information of active sites.

We also measure the activity of some key residues interacting with NADPH. Mutation of Y216, which stacks against the adenine ring of NADPH, shows a great loss of enzyme activity, indicating the critical role of the hydrophilic tyrosine for NADPH stability. Similarly, mutagenesis of I263 and V291, which form strong interactions with the nicotinamide moiety of NADPH, results in a significant loss of activity. Therefore, we infer that most residues in the NADPH-binding groove strengthen the protein−cofactor interaction.

Sequence Alignment. Multiple sequence alignment shows that some active site residues, like N43, Y54, T151, V176, and K341, are conserved in homologous QORs, while differences are also found in some other active site residues. For instance, in the structure of PcQOR, the polar residue R45 replaces the corresponding hydrophobic residue Ile from other homologues and the polar residue C147 replaces the nonpolar residues Leu. In addition, some QORs like Zta1 from S.cerevisiae have been reported to be able to reduce the $\alpha\beta$ double bond of alkenals/alkenones using two adjacent tyrosine residues as catalytic residues. However, in PcQOR, the glutamine replaces one tyrosine in Zta1, implying that PcQOR might not reduce the $\alpha\beta$ double bond of alkenals/alkenones (Figure 7).

CONCLUSIONS

This work reports the structure of the *Pc*QOR−NADPH complex. Computational simulation combined with site-directed mutagenesis and enzymatic activity assays enable us to define the potential quinone-binding site of *Pc*QOR. Based on these, we propose a catalytic mechanism of *Pc*QOR. When quinone enters the active pocket, the substrate will be redistributed by the side chains of R45, Q48, Y54, C147, and T148 and the NADPH nicotinamide ring. Electron transfer proceeds once the phenyl ring of quinone stacks against the nicotinamide ring. The increased hydrophobicity around the positively charged nicotinamide cavity stimulates electron transfer from NADPH to the substrate in the ternary
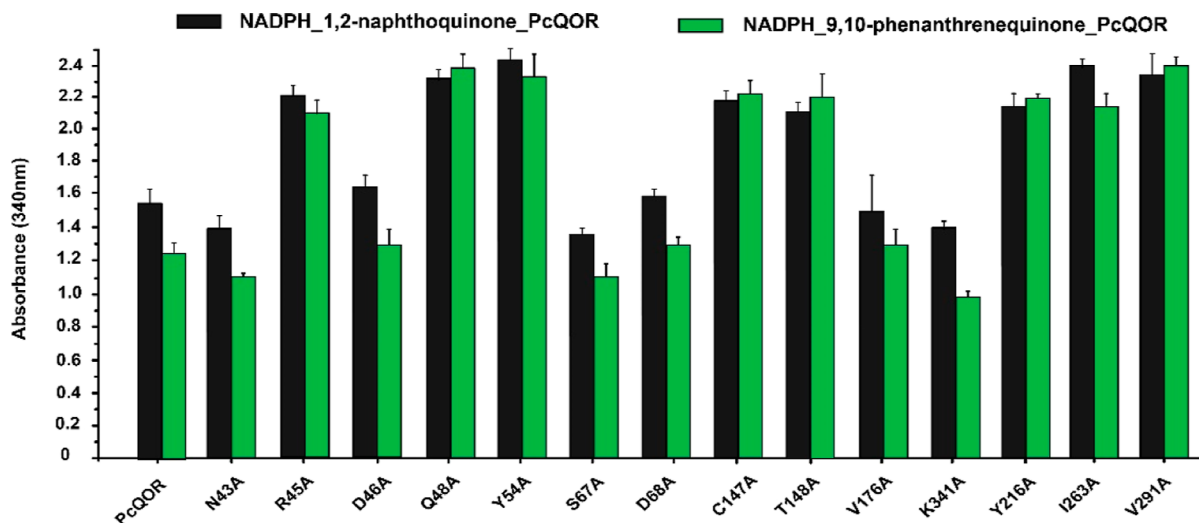
Figure 6. Enzymatic activity of site-directed mutants of *Pc*QOR. Enzyme activity rates were tested by monitoring the decrease in absorbance of NADPH at 340 nm. Mutation of residues that were estimated to interact with substrates exhibited lower enzyme activity than other mutants. Each assay was conducted in triplicate, from which the average ± s.d. was calculated.
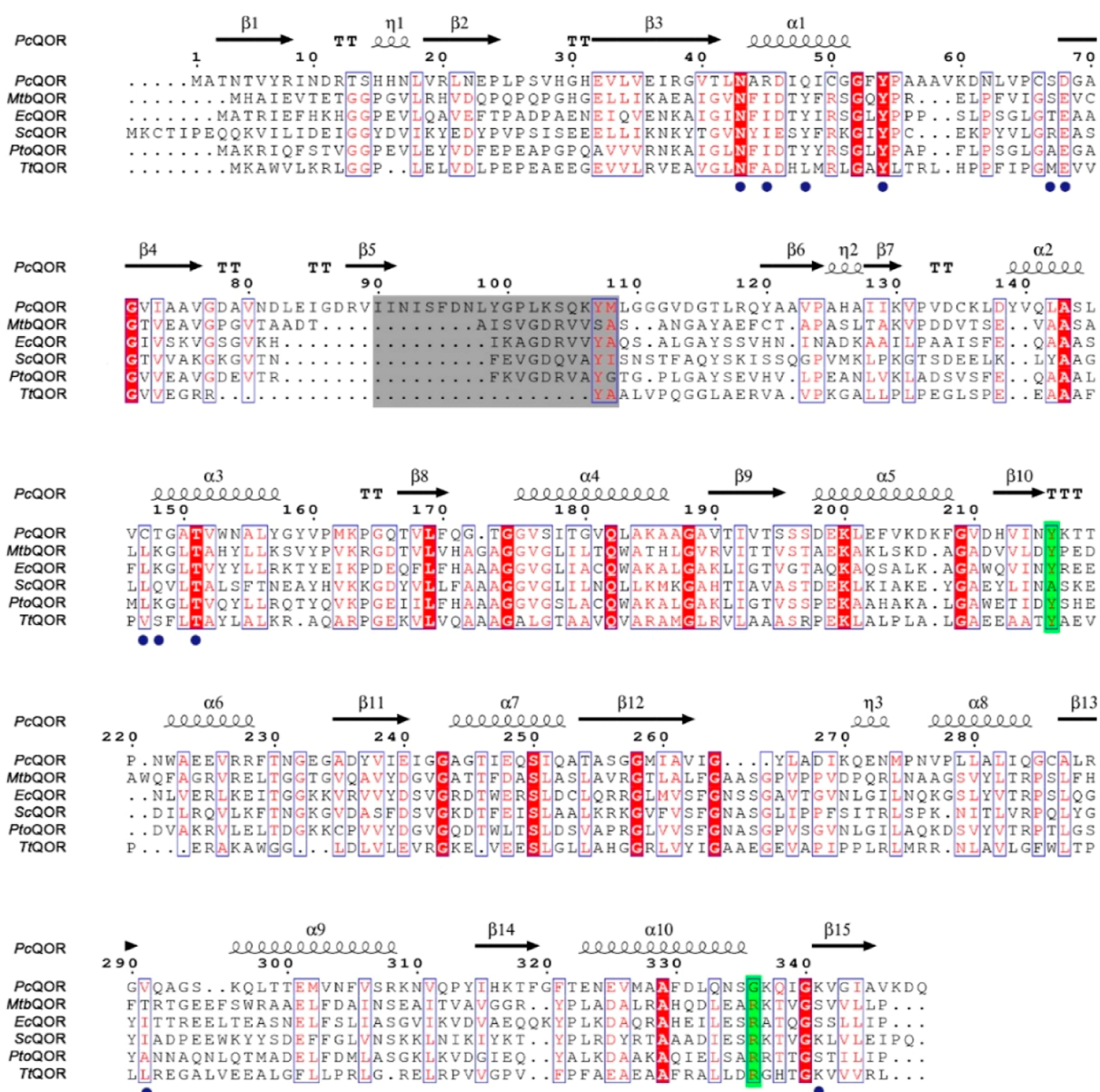
Figure 7. Structure-based sequence alignment of representative QORs. The key substrate-interacting residues are labeled by blue circles. The special loop covering the active pocket of *Pc*QOR is marked by a gray box. Residues that determine the conformation of the adenine ring of NADPH are marked by a green box. Structure-based sequence alignment was created using Clustal X Version 2.0[59] and ESPript 3.0.[60] Reprinted with permission from [Clustal W and Clustal X version 2.0]. Copyright [2007] [Oxford University Press]. Reprinted with permission from [deciphering key features in protein structures with the new ENDscript server]. Copyright [2014] [published by the Oxford University Press on behalf of nucleic acid research].

enzyme−NADPH−substrate complex.[61] After reduction of the quinone carbonyl group, the hydrogen bonds between quinone and the side chain of R45, Q48, and Y54 are broken. As the reduction reaction is complete, the substrate-binding pocket opens to release the product.

■ DATA AVAILABILITY STATEMENT

The atomic coordinates and structure factors of the reported structure have been deposited in the Protein Data Bank under accession codes 7VEM. All other relevant data are available from the corresponding author upon request.

■ ASSOCIATED CONTENT

ⓢ Supporting Information

The Supporting Information is available free of charge at https://pubs.acs.org/doi/10.1021/acsomega.2c02954.

> Sequence alignment of OQRs from some oomycetes, primers used in the study, and mutagenesis oligonucleotides (PDF)

■ AUTHOR INFORMATION

Corresponding Author

Chunyuan Zhu − College of Life Sciences, Shandong Agricultural University, Taian 271018, China; Email: zhuchunyuan@sdau.edu.cn

Authors

Cancan Yang − *Shandong Provincial Key Laboratory for Biology of Vegetable Diseases and Insect Pests, College of Plant Protection, Shandong Agricultural University, Taian 271018, China;* ⊙ orcid.org/0000-0002-9841-3545

Zhenling Huang − *Shandong Provincial Key Laboratory for Biology of Vegetable Diseases and Insect Pests, College of Plant Protection, Shandong Agricultural University, Taian 271018, China*

Xiuguo Zhang − *Shandong Provincial Key Laboratory for Biology of Vegetable Diseases and Insect Pests, College of Plant Protection, Shandong Agricultural University, Taian 271018, China*

Complete contact information is available at:
https://pubs.acs.org/10.1021/acsomega.2c02954

■ REFERENCES

(1) Bolton, J. L.; Trush, M. A.; Penning, T. M.; Dryhurst, G.; Monks, T. J. Role of quinones in toxicology. *Chem. Res. Toxicol.* **2000**, *13*, 135−160.

(2) Qian, L.; Yang, F.; Lin, X.; Jiang, S.; Zhang, Y.; Tang, Y. Pyrroloquinoline quinone ameliorates liver injury in mice induced by cyclophosphamide. *Environ. Sci. Pollut. Res. Int.* **2022**, *29*, 30383−30393.

(3) Dinkova-Kostova, A. T.; Talalay, P. Persuasive evidence that quinone reductase type 1 (DT diaphorase) protects cells against the toxicity of electrophiles and reactive forms of oxygen. *Free Radic. Biol. Med.* **2000**, *29*, 231−240.

(4) Nioi, P.; Hayes, J. D. Contribution of NAD(P)H:quinone oxidoreductase 1 to protection against carcinogenesis, and regulation of its gene by the Nrf2 basic-region leucine zipper and the arylhydrocarbon receptor basic helix-loop-helix transcription factors. *Mutat. Res.* **2004**, *555*, 149−171.

(5) Qiu, D.; Song, S.; Wang, Y.; Bian, Y.; Wu, M.; Wu, H.; Shi, Y.; Duan, H. NAD(P)H: quinone oxidoreductase 1 attenuates oxidative stress and apoptosis by regulating Sirt1 in diabetic nephropathy. *J. Transl. Med.* **2022**, *20*, 44.

(6) Kim, I. K.; Yim, H. S.; Kim, M. K.; Kim, D. W.; Kim, Y. M.; Cha, S. S.; Kang, S. O. Crystal structure of a new type of NADPH-dependent quinone oxidoreductase (QOR2) from Escherichia coli. *J. Mol. Biol.* **2008**, *379*, 372−384.

(7) Feng, Y.; Li, W.; Li, L.; Wang, J.; Ge, J.; Xu, D.; Liu, Y.; Wu, K.; Zeng, Q.; Wu, J. W.; Tian, C.; Zhou, B.; Yang, M. Structural insight into the type-II mitochondrial NADH dehydrogenases. *Nature* **2012**, *491*, 478−482.

(8) Yagi, T. Bacterial NADH-quinone oxidoreductases. *J. Bioenerg. Biomembr.* **1991**, *23*, 211−225.

(9) Pan, X.; Zhang, H.; Gao, Y.; Li, M.; Chang, W. Crystal structures of Pseudomonas syringae pv. tomato DC3000 quinone oxidoreductase and its complex with NADPH. *Biochem. Biophys. Res. Commun.* **2009**, *390*, 597−602.

(10) Guo, P. C.; Ma, X. X.; Bao, Z. Z.; Ma, J. D.; Chen, Y.; Zhou, C. Z. Structural insights into the cofactor-assisted substrate recognition of yeast quinone oxidoreductase Zta1. *J. Struct. Biol.* **2011**, *176*, 112−118.

(11) Kwiek, J. J.; Haystead, T.; Rudolph, J. Kinetic Mechanism of Quinone Oxidoreductase 2 and Its Inhibition by the Antimalarial Quinolines. *Biochemistry* **2004**, *43*, 4538−4547.

(12) Tedeschi, G.; Chen, S.; Massey, V. DT-diaphorase. *J. Biol. Chem.* **1995**, *270*, 1198−1204.

(13) Prestera, T.; Holtzclaw, W. D.; Zhang, Z. P.; Talalay, P. Chemical and molecular regulation of enzymes that detoxify carcinogens. *Proc. Natl. Acad. Sci. U.S.A.* **1993**, *90*, 2965−2969.

(14) Beyer, R. E.; Segura-Aguilar, J.; Di Bernardo, S. D.; Cavazzoni, M.; Fato, R.; Fiorentini, D.; Galli, M. C.; Setti, M.; Landi, L.; Lenaz, G. The role of DT-diaphorase in the maintenance of the reduced antioxidant form of coenzyme Q in membrane systems. *Proc. Natl. Acad. Sci. U.S.A.* **1996**, *93*, 2528−2532.

(15) Li, R. B.; Bianchet, P.; Talalay, L. M.; Amzel, M. A. The three-dimensional structure of NAD(P)H:quinone reductase, a flavoprotein involved in cancer chemoprotection and chemotherapy: mechanism of the two-electron reduction. *Proc. Natl. Acad. Sci. U.S.A.* **1995**, *92*, 8846−8850.

(16) Porté, S.; Moeini, A.; Reche, I.; Shafqat, N.; Oppermann, U.; Farrés, J.; Parés, X. Kinetic and structural evidence of the alkenal/one reductase specificity of human ζ-crystallin. *Cell. Mol. Life Sci.* **2011**, *68*, 1065.

(17) Thorn, J. M.; Barton, J. D.; Dixon, N. E.; Ollis, D. L.; Edwards, K. J. Crystal Structure ofEscherichia coliQOR Quinone Oxidoreductase Complexed with NADPH. *J. Mol. Biol.* **1995**, *249*, 785−799.

(18) Jaiswal, A. K. Characterization and Partial Purification of Microsomal NAD(P)H:Quinone Oxidoreductases. *Arch. Biochem. Biophys.* **2000**, *375*, 62−68.

(19) Oppermann, U. Carbonyl reductases: the complex relationships of mammalian carbonyl- and quinone-reducing enzymes and their role in physiology. *Annu. Rev. Pharmacol. Toxicol.* **2007**, *47*, 293−322.

(20) Porté, S.; Crosas, E.; Yakovtseva, E.; Biosca, J. A.; Farrés, J.; Fernández, M.; Parés, X. MDR quinone oxidoreductases: the human and yeast zeta-crystallins. *Chem. Biol. Interact.* **2009**, *178*, 288.

(21) Huang, Q. L.; Russell, P.; Stone, S. H.; Zigler, J. S. Zeta-crystallin, a novel lens protein from the guinea pig. *Curr. Eye Res.* **1987**, *6*, 725−732.

(22) Garland, D.; Rao, P. V.; Corso, A. D.; Mura, U.; Zigler, J. S., Jr. ζ-Crystallin is a major protein in the lens of Camelus dromedarius. *Arch. Biochem. Biophys.* **1991**, *285*, 134−136.

(23) Persson, B.; Zigler, J.; Jornvall, H. A Super-Family of Medium-Chain Dehydrogenases/Reductases (MDR). Sub-Lines including zeta-Crystallin, Alcohol and Polyol Dehydrogenases, Quinone Oxidoreductases, Enoyl Reductases, VAT-1 and other Proteins. *Eur. J. Biochem.* **1994**, *226*, 15−22.

(24) Nordling, E.; Jörnvall, H.; Persson, B. Medium-chain dehydrogenases/reductases (MDR). *Eur. J. Biochem.* **2002**, *269*, 4267−4276.

(25) Cedergren-Zeppezauer, E.; Samama, J. P.; Eklund, H. Crystal-structure determination of reduced nicotinamide adenine dinucleotide complex with horse liver alcohol dehydrogenase maintained in its apo conformation by zinc-bound imidazole. *Biochemistry* **1983**, *22*, 5761−5772.

(26) Rao, P. V.; Zigler, J. S., Jr. Purification and characterization of zeta-crystallin/quinone reductase from guinea pig liver. *Biochim. Biophys. Acta* **1992**, *1117*, 315.

(27) Gonzalez, P.; Rao, P. V.; Zigler, J. S. Molecular Cloning and Sequencing of ζ-Crystallin/Quinone Reductase cDNA from Human Liver. *Biochem. Biophys. Res. Commun.* **1993**, *191*, 902−907.

(28) Tumminia, S. J.; Vasantha Rao, P. V.; Zigler, J. S.; Russell, P. Xenobiotic induction of quinone oxidoreductase activity in lens epithelial cells. *Biochim. Biophys. Acta* **1993**, *1203*, 251−259.

(29) Shimomura, Y.; Kakuta, Y.; Fukuyama, K. Crystal Structures of the Quinone Oxidoreductase from Thermus thermophilus HB8 and Its Complex with NADPH: Implication for NADPH and Substrate Recognition. *J. Bacteriol.* **2003**, *185*, 4211−4218.

(30) Mano, J.; Yoon, H. J.; Asada, K.; Babiychuk, E.; Inzé, D.; Mikami, B. Crystallization and preliminary X-ray crystallographic

analysis of NADPH: azodicarbonyl/quinone oxidoreductase, a plant ζ-crystallin. *Biochim. Biophys. Acta* **2000**, *1480*, 374−376.

(31) Mano, J.; Babiychuk, E.; Belles-Boix, E. B.; Hiratake, J.; Kimura, A.; Inzé, D.; Kushnir, S.; Asada, K. A novel NADPH:diamide oxidoreductase activity in Arabidopsis thaliana P1 ζ-crystallin. *Eur. J. Biochem.* **2000**, *267*, 3661−3671.

(32) Mano, J.; Torii, Y.; Hayashi, S.; Takimoto, K.; Matsui, K.; Nakamura, K.; Inzé, D.; Babiychuk, E.; Kushnir, S.; Asada, K. The NADPH:Quinone Oxidoreductase P1-ζ-crystallin in Arabidopsis Catalyzes the α,β-Hydrogenation of 2-Alkenals: Detoxication of the Lipid Peroxide-Derived Reactive Aldehydes. *Plant Cell Physiol.* **2002**, *43*, 1445−1455.

(33) Kim, S.-Y.; Mori, T.; Min, F. C.; Furuya, S.; Hakoshima, T. Structural insights into vesicle amine transport-1 (VAT-1) as a member of the NADPH-dependent quinone oxidoreductase family. *Sci. Rep.* **2021**, *11*, 2120.

(34) Wang, Z.; Li, L.; Dong, Y. H.; Su, X. D. Structural and biochemical characterization of MdaB from cariogenicStreptococcus mutansreveals an NADPH-specific quinone oxidoreductase. *Acta Crystallogr., Sect. D: Biol. Crystallogr.* **2014**, *70*, 912−921.

(35) Crosas, E.; Porté, S.; Moeini, A.; Farrés, J.; Biosca, M.; Parés, X.; Fernández, M. R. Novel alkenal/one reductase activity of yeast NADPH:quinone reductase Zta1p. Prospect of the functional role for the ζ-crystallin family. *Chem. Biol. Interact.* **2011**, *191*, 32−37.

(36) Kranthi, B. V.; Natarajan, B.; Rangarajan, P. N. Isolation of a single-stranded DNA-binding protein from the methylotrophic yeast, Pichia pastoris and its identification as zeta crystallin. *Nucleic Acids Res.* **2006**, *34*, 4060−4068.

(37) Lulli, M.; Nencioni, D.; Papucci, L.; Schiavone, N. Zeta-crystallin: a moonlighting player in cancer. *Cell. Mol. Life Sci.* **2020**, *77*, 965−976.

(38) Fernández, M. R.; Porté, S.; Crosas, E.; Barberà, N.; Farrés, J.; Biosca, J. A.; Parés, X. Human and yeast ζ-crystallins bind AU-rich elements in RNA. *Cell. Mol. Life Sci.* **2007**, *64*, 1419−1427.

(39) LaVallie, E. R.; DiBlasio, E. A.; Kovacic, S.; Grant, K. L.; Schendel, P. F.; McCoy, J. M. A Thioredoxin Gene Fusion Expression System That Circumvents Inclusion Body Formation in the E. coli Cytoplasm. *Biotechnology* **1993**, *11*, 187−193.

(40) Minor, W.; Cymborowski, M.; Otwinowski, Z.; Chruszcz, M. HKL-3000: the integration of data reduction and structure solution - from diffraction images to an initial model in minutes. *Acta Crystallogr., Sect. D: Biol. Crystallogr.* **2006**, *62*, 859−866.

(41) Otwinowski, Z.; Minor, W. Processing of X-ray diffraction data collected in oscillation mode. *Methods Enzymol* **1997**, *276*, 307−326.

(42) McCoy, A. J.; Grosse-Kunstleve, A.; Adams, B.; Winn, B.; Storoni, C.; Read, A. Phasercrystallographic software. *J. Appl. Crystallogr.* **2007**, *40*, 658−674.

(43) Winn, M.; Ballard, C. C.; Cowtan, K. D.; Dodson, E. J.; Emsley, K. S.; Evans, P. R.; Keegan, R. M.; Krissinel, E. B.; Leslie, A. G. W.; McCoy, A.; McNicholas, S. J.; Murshudov, G. N.; Pannu, N. S.; Potterton, E. A.; Powell, H. R.; Read, R. J.; Vagin, A.; Wilson, K. S. Overview of theCCP4 suite and current developments. *Acta Crystallogr., Sect. D: Biol. Crystallogr.* **2011**, *67*, 235−242.

(44) Adams, P. D.; Afonine, P. V.; Bunkóczi, G.; Chen, V. B.; Davis, I. W.; Echols, N.; Headd, J.; Hung, L. W.; Kapral, G. J.; Grosse-Kunstleve, R. W.; McCoy, A. J.; Moriarty, N. W.; Oeffner, R.; Read, R. J.; Richardson, D. C.; Richardson, J. S.; Terwilliger, T. C.; Zwart, P. H. PHENIX: a comprehensive Python-based system for macro-molecular structure solution. *Acta Crystallogr., Sect. D: Biol. Crystallogr.* **2010**, *66*, 213−221.

(45) Emsley, P.; Cowtan, K. Coot: model-building tools for molecular graphics. *Acta Crystallogr., Sect. D: Biol. Crystallogr.* **2004**, *60*, 2126−2132.

(46) Terwilliger, T. C.; Klei, H.; Adams, P. D.; Cohn, J. D.; Moriarty, N. W. Automated ligand fitting by core-fragment fitting and extension into density. *Acta Crystallogr., Sect. D: Biol. Crystallogr.* **2010**, *62*, 915−922.

(47) Chen, V. B.; Arendall, W. B.; Headd, J. J.; Keedy, D. A.; Immormino, D. C.; Kapral, G. J.; Murray, L. W.; Richardson, J. S.; Richardson, D. C. MolProbity: All-Atom Structure Validation for Macromolecular Crystallography. *Acta Crystallogr., Sect. D: Biol. Crystallogr.* **2010**, *66*, 12−21.

(48) Delano, W. L. The PyMol Molecular Graphics System. *Proteins* **2002**, *30*, 442−454.

(49) Schuck, P. Size-Distribution Analysis of Macromolecules by Sedimentation Velocity Ultracentrifugation and Lamm Equation Modeling. *Biophys. J.* **2000**, *78*, 1606−1619.

(50) Schuck, P. On the analysis of protein self-association by sedimentation velocity analytical ultracentrifugation. *Anal. Biochem.* **2003**, *320*, 104−124.

(51) Zhao, B.; Guengerich, F. P.; Voehler, M.; Waterman, M. R. Role of Active Site Water Molecules and Substrate Hydroxyl Groups in Oxygen Activation by Cytochrome P450 158A2. *J. Biol. Chem.* **2005**, *280*, 42188−42197.

(52) Adams, P. D.; Grosse-Kunstleve, R. W.; Hung, W. H.; Ioerger, T. R.; McCoy, T. C.; Moriarty, N. W.; Read, R. J.; Sacchettini, J. C.; Sauter, N. K.; Terwilliger, T. C. PHENIX: building new software for automated crystallographic structure determination. *Acta Crystallogr., Sect. D: Biol. Crystallogr.* **2002**, *58*, 1948−1954.

(53) Morris, G. M.; Huey, R.; Lindstrom, W.; Sanner, M. F.; Belew, R. K.; Goodsell, D. S.; Olson, A. J. AutoDock4 and AutoDockTools4: Automated docking with selective receptor flexibility. *J. Comput. Chem.* **2009**, *30*, 2785−2791.

(54) Huey, R.; Morris, G. M.; Olson, A. J.; Goodsell, D. S. A semiempirical free energy force field with charge-based desolvation. *J. Comput. Chem.* **2007**, *28*, 1145−1152.

(55) Rao, P. V.; Krishna, C. M.; Zigler, Z. J. Identification and characterization of the enzymatic activity of zeta-crystallin from guinea pig lens. A novel NADPH:quinone oxidoreductase. *J. Biol. Chem.* **1992**, *267*, 96−102.

(56) Rao, S. T.; Rossmann, M. G. Comparison of super-secondary structures in proteins. *J. Mol. Biol.* **1973**, *76*, 241.

(57) Zheng, Q.; Song, Y.; Zhang, W.; Shaw, N.; Zhou, W.; Rao, Z. Structural views of quinone oxidoreductase fromMycobacterium tuberculosisreveal large conformational changes induced by the co-factor. *FEBS J.* **2015**, *282*, 2697−2707.

(58) Holm, L.; Rosenström, P. Dali server: conservation mapping in 3D. *Nucleic Acids Res.* **2010**, *38*, W545−W549.

(59) Larkin, M. A.; Blackshields, G.; Brown, N. P.; Chenna, R.; McGettigan, P. A.; McWilliam, H.; Valentin, F.; Wallace, I. M.; Wilm, A.; Lopez, R.; Thompson, J. D.; Gibson, T. J.; Higgins, D. G. Clustal W and Clustal X version 2.0. *Bioinformatics* **2007**, *23*, 2947−2948.

(60) Robert, X.; Gouet, P. Deciphering key features in protein structures with the new ENDscript server. *Nucleic Acids Res.* **2014**, *42*, W320−W324.

(61) Eklund, H.; Samama, J. P.; Wallén, L.; Brändén, C.; Åkeson, A.; Jones, T. A. Structure of a triclinic ternary complex of horse liver alcohol dehydrogenase at 2.9 Å resolution. *J. Mol. Biol.* **1981**, *146*, 561−587.